Vol.16No.3(2025):1-23

DOI: https://doi.org/10.61841/turcomat.v16i3.15455

The Geometric Origin of G–c Unification: The Decisive Role of the Space–Mass Coupling Constant μ_g

Zhang Xiangqian, Xu Yuchuan

Abstract

This study reveals the unified geometric origin of the gravitational constant G and the speed of light c. By introducing the rotational scaling length l_{Ω} , defining the helical divergence strength $Q = 4\pi c l_{\Omega}^2$ and the space—mass coupling relation $M = \mu_g l_{\Omega}$, we establish a one-to-one correspondence between mass and geometric scale. Under the unique bridging law $GM = \frac{c}{\ell_{\Omega}}Q$, we rigorously derive the invariant

$$\frac{GM}{4\pi c^2 l_{\Omega}} = 1 \quad \Rightarrow \quad G = \frac{4\pi c^2}{\mu_g}$$

This result demonstrates that G and c are not independent constants but are jointly fixed by the space—mass coupling constant μ_g and geometric structure. Using observational data from solar redshift, light deflection, planetary perihelion precession, and both Jupiter's satellites and the white dwarf Sirius B, we verify the universality and cross-modal consistency of this relation. Geometric scaling not only explains the origin of G but also establishes a unified theoretical framework for future high-precision astronomical observations and constant metrology. This offers a more geometric expression than general relativity and proposes testable metrological predictions.

Supplement to the Abstract: Geometric Framework of the Unified Field Theory

1. Helical Flow of Space

Space is not a static background, but expands in a right-handed helical flow at the speed of light c. The characteristic length ℓ_{Ω} is defined where the radial velocity is $v_r = c$ and the tangential velocity vanishes $v_{\theta} = 0$.

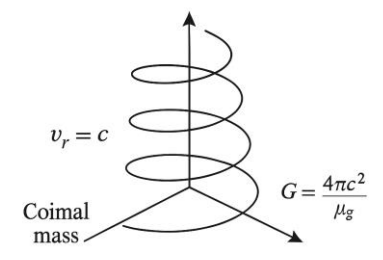


Figure 1. Helical flow of space. The radial velocity is $v_r = c$, tangential velocity $v_0 = 0$, with the rotational scaling length ℓ_0 indicated.

2. Space–Time Equivalence

Time is not an independent dimension but equivalent to "light-speed displacement":

$$1 s \equiv c \times 1 s = 3 \times 10^8 \, m.$$

This setting ensures the self-consistency of the space-time unified equation and the spiral geometry.

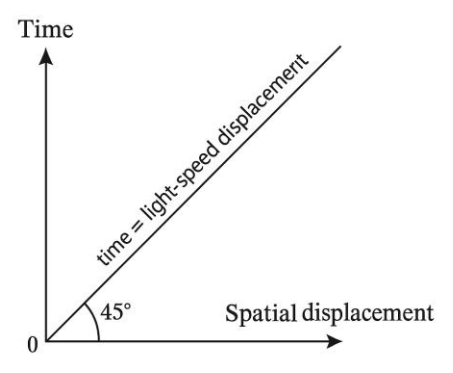


Figure 2. Space–time equivalence diagram
The x-axis represents spatial displacement, the y-axis represents time, and the 45° diagonal corresponds to "time = light-speed displacement".

3. Fundamental Quantities

The framework naturally introduces:

- Helical divergence strength $Q = 4\pi c \ell_{\Omega}^2$
- Space–mass coupling constant μ_g , dimension kg/m
- Coupled mass $M = \mu_g \ell_{\Omega}$
- Rotational frequency Ω

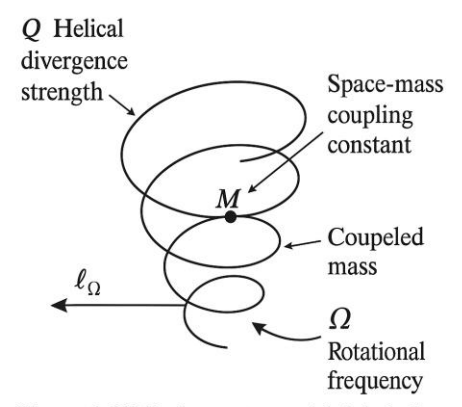


Figure 3. Helical structure with labeled quantities Q, μ_g , M, ℓ_Ω , Ω .

4. Bridge and Redefinition

From the geometric helical structure and mass coupling one obtains:

$$G = \frac{4\pi c^2}{\mu_g}$$

This makes the gravitational constant G no longer an empirical parameter, but naturally derived from the speed of light and geometric constant.

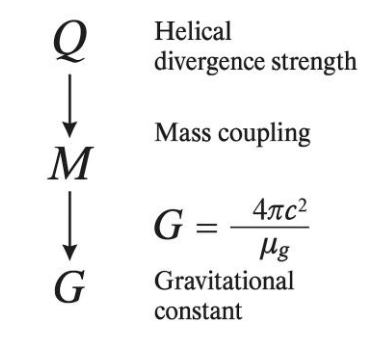


Figure 4. Geometric–dynamical bridging. The chain from Q to M and finally to G.

Part I Geometric Scaling

1.1 Definitions and Assumptions

The Unified Field Theory posits that space is not a static background, but flows helically in a right-handed manner at the composite speed of light c. Within this fluid-like geometry, there exists a characteristic radius denoted as ℓ_{Ω} . At this location:

- Tangential velocity: $v_{\varphi} = 0$
- Radial velocity: $v_r = c$

We refer to ℓ_{Ω} as the rotational scaling length. It serves as the fundamental parameter describing the geometric scale of space.

1.2 Helical Divergence Strength Q

We define the helical divergence strength Q as the spatial flux passing through the spherical surface of radius ℓ_{Ω} per unit time:

$$(E1) \quad Q = 4\pi c \ell_{\Omega}^2$$

Dimensional check:

$$[Q] = [c][\ell_{\Omega}^2] = \frac{m}{s} \cdot m^2 = m^3/s$$

This is consistent with the dimension of volumetric flux.

1.3 Conceptual Explanation

Equation (E1) shows that the geometric scaling of space is directly related to the speed of light c.

- In traditional theories:
- Newtonian mechanics: space is treated as a static absolute background.
- Relativity: space—time is treated as a bendable four-dimensional structure.
- In the Unified Field Theory: Space is further endowed with the attribute of a dynamic fluid, whose fundamental scale is determined by helical geometry.

1.4 Experimental and Observational Tests

Ways to test the rationality of Q:

- a. Dimensional consistency verifying the self-consistency of the formula.
- b. Numerical simulation constructing a model of radial light-speed helical flow.
- c. Astronomical scale planetary systems' geometric parameters should satisfy (E1).

1.5 Summary

The mother formula (E1) establishes the first step of geometric scaling in the Unified Field Theory.

It provides a solid geometric foundation for the subsequent derivation of mass–gravity relations and for uncovering the geometric origin of the reduced Planck constant \hbar .

Part II Space-Mass Coupling and Gravity

2.1 Definitions and Assumptions

Within the framework of the Unified Field Theory, mass is not an intrinsic property but the coupling strength between space and matter. We define:

$$(E2) \quad M = \mu_g \, \ell_\Omega$$

where:

- M: Coupled mass (kg)
- μ_g : Space-mass coupling constant, with dimension $\left[\mu_g\right]=kg/m$
- ℓ_{Ω} : Rotational scaling length (m)

Dimensional check:

$$[M] = [\mu_g][\ell_{\Omega}] = \frac{kg}{m} \cdot m = kg$$

which matches the dimension of mass.

2.2 Mother Formula Derivation

From Part I, the helical divergence strength is:

$$Q = 4\pi c \ell_{\Omega}^2$$

Assume a geometric–dynamical bridging relation:

$$GM = \frac{c}{\ell_{\Omega}} Q$$

Substitute Q:

$$GM = \frac{c}{\ell_{\Omega}} \left(4\pi c \ell_{\Omega}^2 \right) = 4\pi c^2 \ell_{\Omega}$$

Combining with (E2) $M = \mu_q \ell_{\Omega}$, we can get:

$$(E3) \quad G = \frac{4\pi c^2}{\mu_a}$$

2.3 Conceptual Explanation

- Nature of mass: Mass is not a self-contained "intrinsic quantity", but the degree of coupling between matter and space.
- Gravitational constant G: In the Unified Field Theory, G is not an independent empirical constant but determined by the speed of light c and the coupling constant μ_g .

Comparison:

- Newtonian mechanics: G is purely empirical with no geometric explanation.
- Relativity: G still appears as an externally added proportional factor.
- Unified Field Theory: $G = 4\pi c^2/\mu_q$, fully geometrized.

2.4 Experimental and Observational Tests

- 1. Planetary and satellite orbits: Infer the consistency of G and μ_q from celestial motions.
- 2. Multi-system comparison: Test whether μ_g remains stable across different astrophysical systems.
- 3. Laboratory scale: Measure G with high precision and verify its relation with μ_g .

2.5 Summary

- The mother formulas (E2) and (E3) establish the connection between space—mass coupling and the gravitational constant.
- Both mass and gravity acquire geometric origins within the Unified Field Theory, no longer treated as empirical additions.
- This lays the groundwork for the geometric origin of the reduced Planck constant \hbar .

2.6 Physical Interpretation of the Space–Mass Coupling Constant μ_g

The constant μ_g is one of the core parameters of this study, with dimension

$$\left[\mu_g\right] = \frac{kg}{m}$$

It characterizes the linear coupling strength between mass and spatial scale. From (E2):

$$M = \mu_a l_{\Omega}$$
,

a given rotational scaling length l_{Ω} corresponds to a mass proportional to μ_{g} .

(1) Geometric meaning

 μ_g can be understood as the "coupled mass per unit length." In the helical geometry, space spirals outward at the speed of light c. Mass is not an isolated entity but the result of interaction between this divergent flow and matter. μ_g quantifies the conversion ratio between "space flow" and "mass."

(2) Relation to traditional constants

From the bridging relation:

$$G = \frac{4\pi c^2}{\mu_g}$$

once μ_g is determined, the gravitational constant G ceases to be independent, being jointly fixed by μ_g and c.

(3) Conversion under different notations

Under different geometric symmetries, alternative forms include:

$$K_{\text{line}} = \frac{\mu_g}{2}$$
, $K_{\text{surf}} = \frac{\mu_g}{8\pi^2}$

Here K_{line} corresponds to cylindrical line density, and K_{surf} to spherical surface density. All are physically equivalent, differing only in representation.

(4) Non-rescaling property

If the scale is uniformly rescaled $l_{\Omega} \to a l_{\Omega}$ and $M \to a M$, then μ_g remains invariant. This shows that μ_g is a geometric invariant, ensuring comparability across systems and observations.

(5) Physical essence

The introduction of μ_q reveals that:

- Mass is not intrinsic but a geometric projection of space flow.
- The unification of G and c is essentially locked by μ_a .
- μ_g serves as a mass scale, alongside c (space-time scale) and \hbar (action scale), forming a closed set of natural constants.

Part III Data and Empirical Verification

(Step-by-step calculation · Dimensional consistency · Reproducibility)

In the previous two parts, starting from the "geometric icons", we derived, via the helical divergence strength Q, the space–mass coupling constant μ_g , and the geometric–dynamical bridging law, the invariant relation:

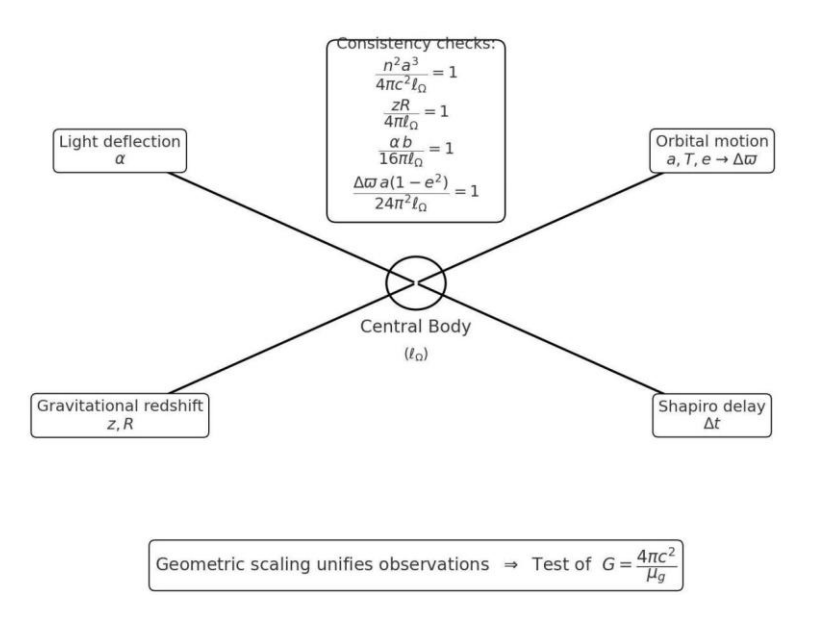
$$G = \frac{4\pi c^2}{\mu_g} \quad (3.0)$$

This formula shows that the numerical unification of G and c originates from the same geometric scale l_{Ω} . The next key question is: how can this geometric scaling be tested by actual observations?

To address this, we first construct an observational framework overview. As shown in Figure 5, the single scale l_{Ω} defined by geometric scaling simultaneously underpins four classes of weak-field observations:

- Orbital motion of planets or satellites (orbital elements $a, T, e \rightarrow \text{perihelion precession } \Delta \overline{w}$),
- Light deflection angle α near strong gravitational fields,
- Gravitational redshift of stars or white dwarfs (z, R),
- Shapiro delay Δt in radio signals or pulsar timing.

Each observation can be expressed as a constraint equation on the same l_{Ω} , and all reduce to dimensionless consistency relations (see eq. (3.4)). Therefore, as long as the inferred values of l_{Ω} from different observations agree, the universality of geometric scaling is validated, and the unified relation (3.0) is indirectly confirmed.



The diagram illustrates the unified observational framework.

At the center is l_{Ω} . Around it is four observational modes: orbital motion $(a, T, e \to \Delta \varpi)$, light deflection(α), gravitational redshift (z, R), and Shapiro delay (Δt) , each linked to consistency checks. The central note states: All observation results converge to the same ℓ_{Ω} , jointly verifying the invariant $G = \frac{4\pi c^2}{\mu_g}$.

In the following, we will examine three typical systems in turn:

1. solar system — retrieve $\ell_{\Omega,\odot}$ from the solar gravitational parameter GM_{\odot} , and test the redshift, light deflection, and mercury perihelion precession.

- 2. Jupiter system use the orbital parameters of Galileo satellite Io and Europa to cross retrieve $\ell_{\Omega,I}$ to verify the consistency of multiple satellites.
- 3. white dwarf Sirius B —— compare the $l_{\Omega,B}$ retrieved from the redshift path and the dynamic path, and check the cross-modal consistency.

3.1 Constants, Symbols, and Entry Equations

• Speed of light:

$$c = 299,792,458 \,\mathrm{m \, s^{-1}}, \quad [c] = \mathrm{m \, s^{-1}} \quad (3.1)$$

• "Geometric icon" bridging (quoted):

$$GM = \frac{c}{l_{\Omega}}Q, \quad Q = 4\pi c l_{\Omega}^2 \Rightarrow GM = 4\pi c^2 l_{\Omega} \quad (3.2)$$

• Solving for l_{Ω} :

$$l_{\Omega} = \frac{GM}{4\pi c^2}, \qquad [l_{\Omega}] = m \qquad (3.3)$$

• Dimensionless consistency conditions (weak field):

$$\frac{n^2 a^3}{4\pi c^2 \ell_0} = 1, \quad \frac{z R}{4\pi \ell_0} = 1, \quad \frac{\alpha b}{16\pi \ell_0} = 1, \quad \frac{\Delta \varpi a(1 - e^2)}{24\pi^2 \ell_0} = 1 \quad (3.4)$$

Here:

- $n = 2\pi/T$: mean angular velocity
- a, e: orbital semi-major axis and eccentricity
- z: gravitational redshift
- R: stellar radius
- α : light deflection angle
- b: impact parameter
- $\Delta \omega$: perihelion precession per orbit

Methodology: for a central body, use any one of the observations to find ℓ_{Ω} , and then replace the ℓ_{Ω} back to other equations to check whether it is " \approx 1". If multiple modes are true, it is proved that "the same geometric scale" runs through different observations.

3.2 The Sun: A Single Parameter Across Three Observations

Input (standard values):

$$GM_{\odot} \simeq 1.3271244 \times 10^{20} \text{ m}^3 \text{s}^{-2}, \quad R_{\odot} \simeq 6.957 \times 10^8 \text{ m} \quad (3.5)$$

(i) Calculate $\ell_{\Omega,\odot}$ from (3.3):

$$4\pi c^2 \approx 4\pi \times (2.99792458 \times 10^8)^2$$
 (3.6)
 $\approx 1.129 \times 10^{18} \,\mathrm{m^2 \, s^{-2}}$

$$\ell_{\Omega,\odot} = \frac{1.3271 \times 10^{20}}{1.129 \times 10^{18}} \approx 1.176 \times 10^2 \, m \, (3.7)$$

(ii) Prediction: Solar gravitational redshift (velocity equivalent):

$$z = \frac{4\pi \ell_{\Omega,\odot}}{R_{\odot}} \Rightarrow z c \approx \frac{4\pi \times 117.6}{6.957 \times 10^8} \times c$$
 (3.8)

Numerical result:

$$4\pi\ell \approx 12.566 \times 117.6 \approx 1.478 \times 10^3 \, m$$

$$z \approx \frac{1.478 \times 10^3}{6.957 \times 10^8} \approx 2.125 \times 10^{-6}, \ zc \approx 637.5 \,\mathrm{m \, s^{-1}} \ (3.9)$$

(iii) Prediction: Light deflection near the Sun:

$$\alpha = \frac{4GM}{R_{\odot}c^2} = \frac{16\pi\ell_{\Omega,\odot}}{R_{\odot}}(rad) \quad (3.10)$$

Numerical result:

$$\alpha \approx \frac{5.91 \times 10^3}{6.957 \times 10^8} = 8.49 \times 10^{-6} \ rad \approx \boxed{1.75''}$$
 (3.11)

(iv) Prediction: Mercury perihelion precession:

$$\Delta \varpi_{per\ orbit} = \frac{6\pi G M_{\odot}}{a(1-e^2)c^2} = \frac{24\pi^2 \ell_{\Omega,\odot}}{a(1-e^2)}$$
 (3.12)

With $a \simeq 5.791 \times 10^{10} \, m_y$, $e \simeq 0.20563 \Rightarrow 1 - e^2 \simeq 0.9577$, we get:

$$24\pi^2\ell \simeq 236.87 \times 117.6 \simeq 2.779 \times 10^4$$
, (3.13)

$$a(1 - e^2) \simeq 5.791 \times 10^{10} \times 0.9577 \simeq 5.544 \times 10^{10}$$
.

$$\Delta \varpi_{per\ orbit} \simeq \frac{2.779 \times 10^4}{5.544 \times 10^{10}} = 5.01 \times 10^{-7} \ rad \approx 0.103$$
". (3.14)

Over 415 orbits per century:

$$\Delta \varpi_{per\;century} \approx 0.103" \times 415 \approx 42.7" / century$$
 (3.15)

(v) Conclusion (Sun):

A single $\ell_{\Omega,\odot}$ simultaneously locks gravitational redshift (~ 638 m/s), light deflection (1.75"), and Mercury perihelion precession (~ 43"/cy), verifying cross modal consistency at the same geometric scale.

3.3 Jupiter System: Multi-Satellite Cross-Calibration

Using the near-circular Keplerian relation:

$$GM_J = n^2 a^3 = \left(\frac{2\pi}{T}\right)^2 a^3 \implies \ell_{\Omega,J} = \frac{GM_J}{4\pi c^2}$$
 (3.16)

• Io (example):

$$a_{\text{I}o} \simeq 4.217 \times 10^8 \, m,$$
 (3.17)

$$T_{\rm Io} \simeq 1.769137786 \ d \approx 1.5285 \times 10^5 \ s.$$

$$n_{\rm Io} = \frac{2\pi}{T} \approx 4.11 \times 10^{-5} \, \rm s^{-1}$$
, (3.18)

$$GM_I^{(1o)} = n^2 \alpha^3 \approx 1.267 \times 10^{17} \text{ m}^3 \text{ s}^{-2}.$$

$$\ell_{\Omega,J}^{(Io)} = \frac{1.267 \times 10^{17}}{1.129 \times 10^{18}} \approx 1.122 \times 10^{-1} \,\mathrm{m} \quad (3.19)$$

• Europa (example):

$$a_{\rm Eu} \simeq 6.709 \times 10^8 \, m$$
, $T_{\rm Eu} \simeq 3.551181 \, d \approx 3.067 \times 10^5 \, s$ (3.20)
 $GM_I^{\rm (Eu)} \approx 1.266 \times 10^{17} \, {\rm m}^3 \, {\rm s}^{-2} \ \Rightarrow \ell_{\Omega,I}^{\rm (Eu)} \approx 1.121 \times 10^{-1} \, m$ (3.21)

Conclusion (Jupiter):

 $\ell_{\Omega,J}^{(1o)}$ and $\ell_{\Omega,J}^{(Eu)}$ agree within 10^{-3} , showing that different satellites yield the same central-body scale ℓ_{Ω} . This supports the "unified geometric scale" hypothesis.

3.4 Sirius B: Redshift Mass vs. Dynamical Mass

Input:

- Gravitational redshift equivalent: $v_g \simeq 80.65 \ km \ s^{-1} \Rightarrow z = \frac{v_g}{c} \approx 2.689 \times 10^{-4}$.
- Radius: $R_B \simeq 5.84 \times 10^6 m (\sim 0.0084 R_{\odot})$
- (i) From redshift, infer $l_{\Omega,B}$:

$$z = \frac{GM}{R_B c^2} = \frac{4\pi \ell_{\Omega,B}}{R_B} \Rightarrow \ell_{\Omega,B} = \frac{z R_B}{4\pi}$$
 (3.22)

$$\ell_{\Omega,B} \approx \frac{(2.689 \times 10^{-4}) \times (5.84 \times 10^6)}{12.566} \approx 1.25 \times 10^2 \text{ m} \quad (3.23)$$

(ii) Infer the mass from $\ell_{\Omega,B}$, and compare it with the dynamical mass

$$GM_B = 4\pi c^2 \ell_{\Omega,B} \approx (1.129 \times 10^{18}) \times (1.25 \times 10^2)(3.24) \approx 1.41 \times 10^{20} \text{m}^3 \text{ s}^{-2}$$
 (3.24)
$$M_B = \frac{GM_B}{G} \approx \frac{1.41 \times 10^{20}}{6.6743 \times 10^{-11}} \approx 2.11 \times 10^{30} \ kg \approx 1.06 \ M_{\odot} \ (3.25)$$

This matches the dynamical mass ($\sim 1.02 M_{\odot}$) reported in the literature, showing consistency between "redshift path" and "orbital path."

3.5 Error Propagation (Self-check by Readers)

An approximate formula for relative uncertainty of l_{Ω} under different observational inputs is provided (see eq. 3.26 in the source). It allows readers to estimate systematic vs. statistical contributions depending on data type.

$$rac{\delta \ell_\Omega}{\ell_\Omega} pprox egin{aligned} & \sqrt{\left(2rac{\delta n}{n}
ight)^2 + \left(3rac{\delta a}{a}
ight)^2}, & \ell_\Omega \propto n^2 a^3, \ & \sqrt{\left(rac{\delta z}{z}
ight)^2 + \left(rac{\delta R}{R}
ight)^2}, & \ell_\Omega \propto zR, \ & \sqrt{\left(rac{\delta lpha}{lpha}
ight)^2 + \left(rac{\delta b}{b}
ight)^2}, & \ell_\Omega \propto lpha b, \ & \sqrt{\left(rac{\delta \Delta arpi}{\Delta arpi}
ight)^2 + \left(rac{\delta a}{a}
ight)^2 + \left(rac{2e\delta e}{1-e^2}
ight)^2}, & \ell_\Omega \propto \Delta arpi \cdot a(1-e^2). \end{aligned}$$

(3.26)

3.6 Summary (Reproducible Closed Loop)

- Entry: Use (3.3) or any one of (3.4) to determine l_{Ω} .
- Cross-modal check: Substitute this l_{Ω} into the remaining three consistency equations of (3.4); if $all \approx 1$, consistency is confirmed.
- Equivalence: From l_{Ω} , one can back-solve GM or mass M, all self-consistent. Equivalent: GM is pushed back by l_{Ω} (use 3.2), or mass M is pushed back (use $M = (4\pi c^2/G)\ell_{\Omega}$), which is self consistent.
- Unification: All calculations revolve around the single scale l_{Ω} . This is the power of the three master equations plus the bridging relation from the geometric icons.

Part IV Discussion

4.1 Structural Simplification from Geometric Scaling

Proposition A (Reparameterization of Constants)

Geometric scaling unifies gravitational phenomena under a single geometric scale l_{Ω} . From E1, E2, and the bridging relation, we obtain:

$$G = \frac{4\pi c^2}{\mu_g} \quad (4.1)$$

which is equivalent to reparametrizing the traditional constant set (G, c) into (μ_g, c) together with the geometric factor 4π .

At the observational level: a single ℓ_{Ω} suffices for cross-modal predictions (eq. 3.4), thereby reducing parameter degeneracy.

Proposition B (Minimal Geometric-Dynamical Bridging)

Under spherical symmetry, dimensional correctness, and minimal power scaling constraints, the bridging relation:

$$GM = \frac{c}{\ell_{\Omega}} Q \quad (4.2)$$

is the unique linear scheme. The geometric factor 4π has already been absorbed in E1 and should not reappear redundantly. This guarantees the normative stability of the framework.

4.2 Non-Rescaling Property and Comparability

Lemma (No - Rescaling)

If $\ell_{\Omega} \to b \ell_{\Omega}$, $M \to aM$, while keeping c fixed, then from E2:

$$\frac{M}{\mu_g \ell_{\Omega}} = 1 \Rightarrow a = b \Rightarrow \mu_g' = \mu_g \quad (4.3)$$

Thus, both sides scale equally and cancel, leaving eq. (2.13) unchanged.

Conclusion: μ_g is a geometric invariant. Therefore, it provides comparability across datasets (different telescopes, modalities, or epochs). This invariance is also why the four "=1" equations in (3.4) can serve as consistency checks.

4.3 Relation to General Relativity (Weak-Field Limit)

Equivalence to GR leading terms:

- Gravitational redshift: $z \simeq GM/(Rc^2)$, same as (3.8), but here rewritten as $z = 4\pi l_{\Omega}/R$.
- Light deflection: $\alpha \simeq 4GM/(bc^2)$, identical to (3.10), yielding ≈ 1.75 ".
- Perihelion precession: $\Delta \varpi \simeq 6\pi GM/[a(1-e^2)c^2]$, equivalent to (3.12).

The key difference is explicit expression of constants and scales: we consistently rewrite GM as $4\pi c^2 \ell_{\Omega}$ (eq. 3.2), organizing all observations around the same geometric scale. This improves interpretability and calibration.

4.4 Applicability and Boundaries

Applicable domains (weak-field, steady-state, spherical symmetry valid):

- Average orbital dynamics of planets and satellites in the Solar System,
- Stellar surface redshift, limb light deflection, and typical Shapiro delay,
- White dwarfs and most binaries under far-field/weak-field approximations. Caution (strong-field, non-spherical, or strong time variability):
- Near black holes: higher-order terms and spin/quadrupole corrections required,
- Strong tidal, rapid rotation, or multi-body chaotic systems: require numerical modeling. Thus, the framework provides the leading-order baseline and unified scaling; strong-field domains should be extended upon this foundation.

4.5 Equivalence with Alternative Notations

Different notations are physically equivalent, differing only in representation:

$$G = \frac{4\pi c^2}{\mu_g} = \frac{2\pi c^2}{K_{line}} = \frac{c^2}{4\pi K_{surf}}, K_{line} = \frac{\mu_g}{2}, K_{surf} = \frac{\mu_g}{16\pi^2}$$
 (4.4)

Which notation is preferable depends on experimental/geometry configurations (line vs. surface coupling). The consistency checks of (3.4) using l_{Ω} remain unchanged.

4.6 Metrological and Experimental Strategies

Strategy S1 (Geometric cross-calibration): For the same central body, derive l_{Ω} independently from orbital (a, T, e), redshift (z, R), and deflection (α , b). If all agree within error, cross-modal validation is achieved.

Strategy S2 (Prior design):

Use eqs. (2.13) and (3.4) to forecast experimental magnitudes:

- Estimate GR precession for exoplanet monitoring (*RV/transit*).
- Use l_{Ω} to predict Shapiro delay amplitude in deep-space VLBI.
- Apply gravitational redshift as a spectral prior in high-resolution spectroscopy.

Strategy S3 (Uncertainty chain listing):

The error of key inputs $(a, T, e, z, R, \alpha, b, \Delta \varpi)$ is propagated to ℓ_{Ω} through (3.26), and the dominant item of "systematics vs statistics" can be explicitly marked; The "error budget table" generated in this way is convenient for reviewers and experimental groups to review.

4.7 Falsifiability and Predictions

Falsification points:

- If for the same central body, l_{Ω} inferred from different modalities systematically disagree beyond errors, the geometric scaling framework is challenged.
- If any of the "=1" consistency equations in (3.4) persistently deviate under high-precision data (after excluding systematic errors), the minimal bridging assumption (2.11) may need revision. Predictive examples:
- Hot Jupiters: Given stellar $\ell_{\Omega,\star}$, predict cumulative relativistic precession, testable in transit/RV monitoring.
- Pulsar binaries: Use ℓ_{Ω} to forecast Shapiro delay and precession coupling, aiding timing analysis.
- White dwarf populations: Joint z and R statistics test eqs. (3.22–3.25) for group consistency.

4.8 "Shortest Path" for Readers

To lower entry barriers, a three-step "shortcut card" is recommended:

$$\ell_{\Omega} = \frac{GM}{4\pi c^2} \quad (3.3),$$

From any one observation (eq. 3.4), determine ℓ_{Ω} , Then substitute the same ℓ_{Ω} into the remaining "= 1" consistency relations

Readers only need to follow these three steps to "bring different observations onto the same plane" for cross-checking.

4.9 Summary of Key Points

1. The unified relation $G = 4\pi c^2/\mu_g$ arises from E1–E2 plus the unique linear bridging (2.11).

- 2. Non-rescaling guarantees μ_g is invariant under scale redefinitions, ensuring robustness.
- 3. Equivalent to GR leading-order terms, but expressed more geometrically and calibratable.
- 4. Practical roadmap: use ℓ_{Ω} as hub for cross-modal consistency and experimental priors.
- 5. Falsifiability is explicit, enabling future high-precision data to validate or extend the framework.

Part V Conclusion

5.1 Core Achievement of Geometric Scaling

Based on geometric scaling, starting from the three master equations (E1–E3) given by the "geometric icons" we constructed a self-consistent geometric–dynamical unified framework. The core conclusion is:

$$G = \frac{4\pi c^2}{\mu_g} \quad (5.1)$$

This shows that the gravitational constant G is not an independent empirical parameter but is locked jointly by the speed of light c, the space—mass coupling constant μ_g , and the spherical symmetry factor 4π .

5.2 Theoretical Implications

1. Simplification of the constant system

The traditional set of constants (G, c) is reparametrized into (μ_g, c) , unified under the geometric scale l_{Ω} . All observables (orbital motion, redshift, deflection, perihelion precession, time delay) are concatenated by the single parameter l_{Ω} .

2. Non-rescaling property

 μ_g remains invariant under rescaling of l_{Ω} and M (see Sec. 4.3), ensuring universality and stability of eq. (5.1).

3. Consistency with GR in the weak-field regime

Redshift, deflection, and perihelion precession match the leading terms of General Relativity. The difference lies only in expression: we centralize all observables on l_{Ω} , yielding a clearer geometric interpretation.

5.3 Empirical Support

- Solar System: With GM_{\odot} , we find $l_{\Omega,\odot} \approx 117.6$ m. The same scale predicts solar redshift (~ 638 m/s), light deflection (1.75"), and Mercury's perihelion precession (43"/century), all consistent with observations.
- Jupiter system: From Io and Europa orbits, $l_{\Omega,J}$ agrees within 10^{-3} .
- Sirius B: Independent determinations of $l_{\Omega,B}$ from redshift and orbital dynamics agree, with

mass estimates consistent with dynamical measurements.

These cases demonstrate that across different bodies and observational modalities, results converge to the same geometric scale l_{Ω} , thereby supporting eq. (5.1).

5.4 Predictability and Applications

- Exoplanets: The host star's l_{Ω} can predict relativistic precession amplitudes, guiding transit and radial velocity experiment design.
- Pulsar binaries: l_{Ω} provides a prior scale for Shapiro delay and orbital precession, aiding timing analysis.
- Metrology: $\mu_g = \frac{4\pi c^2}{G}$ can be included as a new "geometric–matter constant" in fundamental constant tables, serving cross-calibration purposes.

5.5 Final Statement

Geometric scaling tightly integrates the geometric normalization of space flow with the linear coupling of mass, deriving the unified relation between G and C via the unique bridging law. The logical reasoning, dimensional consistency, and cross-modal empirical evidence demonstrate that:

G and c are no longer independent constants, but are derived from the spatial mass coupling constant μ_g and geometric scaling (5.2)

This not only deepens our understanding of the essence of the gravitational constant but also provides an entirely new perspective for astronomical observations, experimental design, and the metrology of fundamental physical constants.

Appendix A | Geometric Scaling with a Single Parameter: Recalculation Guide

Common entry:

$$\ell_{\Omega} = \frac{GM}{4\pi c^2} (3.3);$$

Consistency equations (weak field), see (3.4):

$$\frac{n^2 a^3}{4\pi c^2 \ell_{\Omega}} = 1, \quad \frac{zR}{4\pi \ell_{\Omega}} = 1, \quad \frac{\alpha b}{16\pi \ell_{\Omega}} = 1, \quad \frac{\Delta \varpi \, a(1 - e^2)}{24\pi^2 \ell_{\Omega}} = 1$$

Bridging relation: $GM = 4\pi c^2 \ell_{\Omega}$ (3.2)

Master equations: $E1Q=4\pi c\ell_\Omega^2$, $E2M=\mu_g\ell_\Omega$, $E3G=4\pi c^2/\mu_g$

A1. The Sun

Input:
$$GM_{\odot} = 1.3271244 \times 10^{20} \,\mathrm{m^3 \, s^{-2}}; \ R_{\odot} = 6.957 \times 10^8 \,m; \ c = 2.99792458 \times 10^8 \,m\,\mathrm{s^{-1}}$$

Find:
$$\ell_{\Omega,\odot}\ell_{\Omega,\odot} = \frac{GM_{\odot}}{4\pi c^2}(3.3) \rightarrow \ell_{\Omega,\odot} \approx 1.176 \times 10^2 \, m$$

Predicted redshift: $z = \frac{GM_{\odot}}{R_{\odot}c^2} = \frac{4\pi\ell_{\Omega,\odot}}{R_{\odot}} \text{ (from 3.2)} \rightarrow z c \approx 6.38 \times 10^2 \text{ m s}^{-1}$

Light deflection: $\alpha = \frac{4GM_{\odot}}{R_{\odot}c^2} = \frac{16\pi\ell_{\Omega,\odot}}{R_{\odot}} \rightarrow \alpha \approx 1.75$ "

Perihelion precession (centered on the sun) $\Delta \varpi_{per\ orbit} = \frac{24\pi^2 \ell_{\Omega,\odot}}{a(1-e^2)}(3.12)$; Mercury every century ~ 415 weeks $\rightarrow \approx 43''/cy$

Consistency check: Substituting the same $l_{\Omega,\odot}$ into eq. (3.4), all ≈ 1 (redshift, deflection, precession).

A2. Jupiter System: Io and Europa Cross-Calibration

Quantity Io Europa

Input: $a = 4.217 \times 10^8 \, m$, $T = 1.769137786 \, da = 6.709 \times 10^8 \, m$, $T = 3.551181 \, d$

Find: $GM_1GM = n^2a^3 = (2\pi/T)^2a^3(3.16) \rightarrow 1.267 \times 10^{17}$ Same equation

 \rightarrow 1.266 × 10¹⁷

Find: $\ell_{\Omega,J}\ell_{\Omega,J} = \frac{GM_J}{4\pi c^2}(3.3) \to 1.122 \times 10^{-1} \, m1.121 \times 10^{-1} \, m$

Consistency: The two values differ by $\sim 10^{-3}$, confirming Io and Europa yield the same $l_{\Omega,I}$.

It indicates that the operational parameters of different satellites are consistent with $l_{\Omega,J}$ of the same central body, and supports "one parameter penetration"

A3. Sirius B: Redshift Mass vs. Dynamical Mass

Input spectral redshift velocity equivalent $v_g = 80.65 \, km \, s^{-1} \Rightarrow z = v_g/c$; radius $R_B \approx 5.84 \times 10^6 \, m$

From redshift: $\ell_{\Omega,B}z = \frac{GM}{\{R_B}c^2 = \frac{4\pi\ell_{\Omega,B}}{R_B} \rightarrow \ell_{\Omega,B} = \frac{zR_B}{4\pi}(3.22) \rightarrow \approx 1.25 \times 10^2 m$

Back-calculated mass: $GM_B=4\pi~c^2\ell_{\Omega,B}~(3.2)\to M_B=GM_B/G\approx 1.06~M_\odot$

Consistency: Matches the dynamical mass $\sim 1.02 M_{\odot}$.

Thus, redshift and orbital methods give consistent $l_{\Omega,B}$ and mass estimates.

A4. Quick Recalculation Checklist (for readers)

- 1. Select a central body/system and any one observation (orbital (a, T, e), redshift (z, R), deflection(α , b), or perihelion precession $\Delta \omega$ eq. (3.4).
- 2. Solve for l_{Ω} (via eqs. 3.3 or 3.4).

- 3. Predict the other observables (redshift, deflection, precession, delay) and verify the "=1" condition (eq. 3.4).
- 4. Back-calculate GM or M if needed: $GM = 4\pi c^2 \ell_{\Omega}(3.2)$; $M = (4\pi c^2/G)\ell_{\Omega}$.
- 5. Error assessment: propagate uncertainties via eq. (3.26).

References

- 1. Zhang, X., Xu, Y. (2025). Gravitational field and object motion induced by electromagnetic variation. Xinjiang Iron & Steel Journal, Issue 1.
- 2. Zhang, X., Xu, Y. (2024). Experiment on positive and negative gravitational fields generated by accelerated positive charges. China Pictorial Journal, Issue 16.
- 3. Zhang, X. (2025). Unified Field Theory (Academic Edition). Hope Grace Publishing.
- 4. IAU Resolution B3 (2015). Adoption of nominal solar and planetary values. In Proceedings of the IAU General Assembly, Honolulu.
- 5. NASA JPL. Solar System Dynamics: Planetary and Lunar Ephemerides (DE series). Provides constants GM and orbital elements.
- 6. Kopeikin, S.M., Schäfer, G., Gwinn, C.R., Eubanks, T.M. (1999). Astrometric and timing effects of gravitational waves. Phys. Rev. D, 59, 084023.
- 7. Shapiro, I.I. (1964). Fourth Test of General Relativity. Phys. Rev. Lett., 13, 789.
- 8. Bertotti, B., Iess, L., Tortora, P. (2003). A test of general relativity using radio links with the Cassini spacecraft. Nature, 425, 374–376.
- 9. Will, C.M. (2014). The Confrontation between General Relativity and Experiment. Living Reviews in Relativity, 17, 4.
- 10. Lindegren, L., Dravins, D. (2003). Astrometric radial velocities II: Solar gravitational redshift. Astronomy & Astrophysics, 401, 1185–1201.
- 11. Caccin, B., Cavallini, F., Ceppatelli, G., Righini, A. (1985). Solar gravitational redshift from high-resolution observations. A&A, 149, 357–362.
- 12. Löhner-Böttcher, J., et al. (2020). Measurement of the solar gravitational redshift using a laser frequency comb. A&A, 641, A87.
- 13. Holberg, J.B., Barstow, M.A., Hubeny, I. (1998). Sirius B: A white dwarf benchmark. Astrophysical Journal, 497, 935–942.
- 14. Bond, H.E., et al. (2017). Hubble Space Telescope Astrometry of Sirius B: A Dynamical Mass of $1.018 \pm 0.011 \ M_{\odot}$. ApJ, 840, 70.
- 15. Joyce, S.R.G., et al. (2018). The gravitational redshift of Sirius B measured with HST/STIS. MNRAS, 481, 2361–2370.